Int J Thermophys (2009) 30:1329–1342
DOI 10.1007/s10765-009-0617-z

Gas Pressure Dependence of the Heat Transport in Porous Solids with Pores Smaller than 10 μm

K. Swimm · G. Reichenauer · S. Vidi · H.-P. Ebert

Received: 15 October 2008 / Accepted: 25 June 2009 / Published online: 9 July 2009

Abstract To elucidate the gaseous heat transfer in open porous materials with pore sizes below 10 μm, an experimental setup for hot-wire measurements at high gas pressures was designed and tested. The samples investigated were organic, resorcinol–formaldehyde-based aerogels with average pore sizes of about 600 nm and 7 μm. The range in gas pressure covered was 10 Pa to 10 MPa. To avoid effects due to mass transport along the inner surface of the porous backbone of the samples, He and Ar, i.e., gases with very low interaction with the sample surface at ambient temperature, were chosen. The study reveals a significant contribution of coupling effects to the thermal transport in nanoporous media. A model has been developed that qualitatively describes the observed gas pressure dependence of the heat transport.

Keywords Aerogels · Coupling effect · Gas pressure · Thermal conductivity

1 Introduction

Porous solids with an average pore size below 10 μm, such as organic or inorganic aerogels, are well known for their excellent thermal insulation performance [1]. This is due to their high porosity and the fact that transport via the gas phase is partially suppressed.

K. Swimm (✉) · G. Reichenauer · S. Vidi · H.-P. Ebert
Functional Materials for Energy Technology, Bavarian Center for Applied Energy Research, Am Hubland, 97074 Würzburg, Germany
e-mail: Swimm@zae.uni-wuerzburg.de

Zeng et al. [2] developed an analytical solution for the gaseous thermal conductivity within the pores of an aerogel up to 10 MPa,

$$\lambda_g = \frac{1}{12}(9\gamma - 5)\sqrt{\frac{8M}{\pi R_m}}c_V \frac{\Phi}{0.25 S_{BET}\rho_a/\Phi + 1/l_g}\frac{p_g}{\sqrt{T}}, \quad (1)$$

where γ is the adiabatic exponent, M is the molar mass, R_m is the universal gas constant, S_{BET} is the specific surface area, ρ_a is the aerogel density, T is the temperature, and Φ is the porosity. Coupling effects were not taken into account. To date no experimental data for the thermal conductivity of an aerogel at pressures above 0.1 MPa are available to check the validity of the theoretical approach.

The aim of this work is, therefore, to provide experimental data as well as a theoretical description of the thermal conductivity of organic aerogels, i.e., resorcinol–formaldehyde (RF) aerogels, at gas pressures above 0.1 MPa. RF-aerogels were used as model systems, because they can be synthesized with different well-defined average pore sizes. For practical reasons, related to the pressure range required, a minimum pore size on the order of 1 μm had to be chosen. Within the framework of this paper, all sol–gel-derived highly porous solids are called "aerogels," independent of their pore size and the drying method applied.

The results of this study are also important for future optimization of the materials with respect to their thermal properties at different environmental conditions. Furthermore, experimentally derived thermal conductivity values over a wide gas pressure range can be used to deduce information about mean pore size and pore size distribution of the porous system investigated [3].

2 Theory

2.1 Contributions to the Total Effective Thermal Conductivity in Aerogels

Aerogels are amorphous highly porous materials consisting of a three-dimensionally interconnected solid backbone which is based on chains of primary particles (see Fig. 1) [4]. The space in between these chains represents the so-called meso- or macropores. The heat transfer in these materials is determined by heat transfer via the solid backbone, radiative heat transfer, and heat transfer via the gas phase in the pores [5]. The thermal conductivity via the solid phase, λ_s, depends on the backbone morphology, its chemical composition, the density of the primary particles, and the connectivity of the backbone. The radiative heat transfer within an aerogel sample can be described as a diffusion process as long as the mean free path of the photons within the relevant wavelength regime is small compared to the extension of the sample in the direction of the temperature gradient; for infrared opacified aerogels, the mean free path is smaller than several micrometers.

At moderate temperatures and atmospheric conditions, heat transfer via the gaseous phase within aerogels is well described [3,5]. Generally, the effective thermal conductivity λ_g of the gas within a porous material with a uniform pore size D as a function of gas pressure p_g can be described by

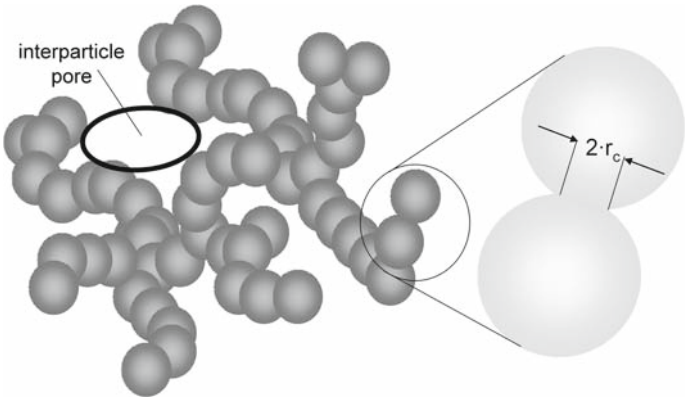

Fig. 1 Sketch of the three-dimensional network of an aerogel consisting of interconnected chains of primary particles. Between two adjacent primary particles, a thermal contact resistance occurs due to the constriction of the heat flux in the surroundings of the contact area with radius r_c

$$\lambda_g(p_g, T) = \Phi \frac{\lambda_{g,0}(p_g, T)}{1 + 2\beta(T) l_g(p_0, T) p_0 / \left[p_g(T) D\right]}, \tag{2}$$

where $\lambda_{g,0}$ is the thermal conductivity of the free gas, β is a coefficient, which depends on the accommodation coefficient and the adiabatic coefficient of the gas [6], l_g is the mean free path of the gas molecules, and p_0 is the reference gas pressure. The thermal conductivity of the free gas can be described by the gas diffusion model,

$$\lambda_{g,0}(p_g, T) = \frac{1}{3} \rho_g(p_g, T) c_V(T) \bar{v}(T) l_g(p_g, T), \tag{3}$$

where ρ_g is the gas density, c_V is the specific heat at constant volume, and $\bar{v}$ is the mean particle velocity.

For porous materials where the solid phase is given by an agglomeration of single or partially interconnected particles (e.g., spheres or fibers) with a relative high bulk thermal conductivity compared to the thermal conductivity of the pore gas, the heat transfer mechanisms via the solid and gaseous phases may interact. This coupling effect is very pronounced within beds of spherical particles and fibrous materials where more or less ideal point contacts between the particles, and thus a high thermal resistance at these contacts, are responsible for the low effective solid thermal conductivity of the solid phase [6].

In many cases, the total heat transfer within porous, optically thick materials can be described by the superposition of the single heat transfer mechanisms leading to the following expression for the total effective thermal conductivity:

$$\lambda_{eff}(T, p_g) = \lambda_s(T) + \lambda_r(T) + \lambda_g(T, p_g) + \lambda_c(\lambda_s, p_g), \tag{4}$$

where λ_r is the radiative thermal conductivity and λ_c is the fraction of the thermal conductivity caused by the coupling effect.

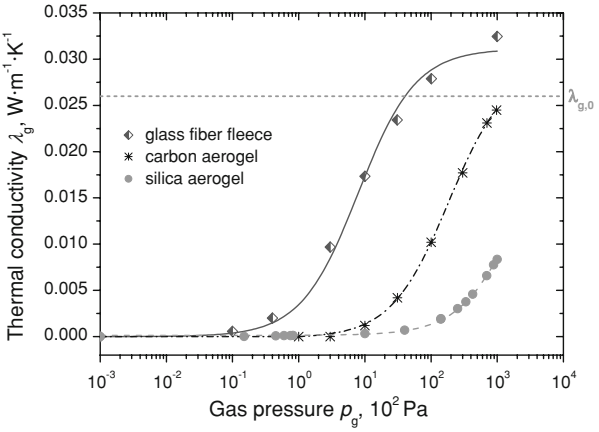

Fig. 2 Experimental gaseous thermal-conductivity values for different porous materials as a function of gas pressure. The data were taken at room temperature in N_2 atmosphere. Lines represent fits of Eq. 2 to the data points

While the coupling effect is well investigated for macroscopically structured materials, it is not discussed yet for materials with pores <10 μm; this is due to the fact that it cannot be observed or well separated from other contributions under standard measurement conditions. The gaseous heat transfer at ambient pressure in materials with pores well below 10 μm, such as aerogels, is controlled by the fact that the mean free path of the gas molecules at ambient conditions is larger than the effective pore dimension. This leads to a thermal conductivity via the gas phase that is smaller than the value of the free gas resulting in very low overall effective thermal-conductivity values for this type of material [7,8].

Figure 2 shows the experimentally determined gaseous thermal conductivities λ_g as a function of gas pressure at ambient temperature for a macroporous glass fiber sample and aerogels with different average pore sizes below 1 μm. For the glass fiber sample, a coupling effect can easily be identified since the gaseous thermal conductivity at ambient air pressure is about $0.032\,\mathrm{W \cdot m^{-1} \cdot K^{-1}}$ which is significantly higher than the thermal conductivity of free air at 300 K, i.e., $0.026\,\mathrm{W \cdot m^{-1} \cdot K^{-1}}$. However, for the aerogels, a coupling effect cannot be identified in the experimental range investigated; this effect is rather expected to become significant at higher gas pressures. Under these conditions, the thermal contact resistances between the primary particles of the network can be bridged by heat transfer within the gas in the immediate proximity of the contact area.

2.2 Modeling of Coupling Effect in Aerogels

A theoretical model, hereafter denoted as aerogel model (AM), was developed to quantify the overall heat transfer through aerogels as a function of the gas pressure within the pores. The new model is based on an existing model introduced by Zehner and Schlünder [9] that describes the heat flow through close-packed particle beds.

As aerogels are highly porous with a large amount of interparticle pore volume, the Zehner model has to be modified.

The total experimentally determined thermal conductivity is given by Eq. 4, where the terms, $\lambda_s + \lambda_r$, correspond to the offset of the measured s-curves in the low gas pressure range where the gaseous thermal conductivity is totally suppressed. The gaseous contribution to the heat transport $\lambda_{g,pore}$ in the interparticle pores can be calculated via Eq. 2, when the porosity and the average pore diameter D_{pore} of the samples are given. The used porosity Π is related to the interparticle pores only, which means that the porosity Φ derived from measurements was corrected by the volume of the small gaps V_{gap} between the primary particles,

$$\begin{aligned} &\frac{\text{Volume of spherical particle, } V_{part}}{\text{Volume of cylindrical unit cell, } V_{cell}} = \frac{2}{3} \\ &\Rightarrow V_{gap} = \frac{1}{3} V_{cell} \Rightarrow V_{gap} = \frac{1}{2} V_{part} \\ &\Rightarrow \Pi = \Phi - (1 - \Phi)\frac{1}{2} = \frac{1}{2}(3\Phi - 1). \end{aligned} \tag{5}$$

The coupling term λ_c can be calculated using Zehner's cylindrical unit cell (Fig. 3); coupling occurs in the small gaps between two adjacent primary particles. The coupling effect is due to a short circuit for the heat flow from one particle to the other via the gas in the gap unless the gaseous heat transfer is completely suppressed. The gap size, which is the distance between the particle surfaces in the direction of the temperature gradient, rises with increasing distance from the central axis.

The aerogel model is based on a cylindrical unit cell (see Fig. 3) which is divided into 1000 hollow cylinders with a constant wall thickness. It is assumed that the heat transport is strictly parallel in each of the hollow cylinders. Mathematically, the coupling effect can then be accounted for by a series connection of the thermal resis-

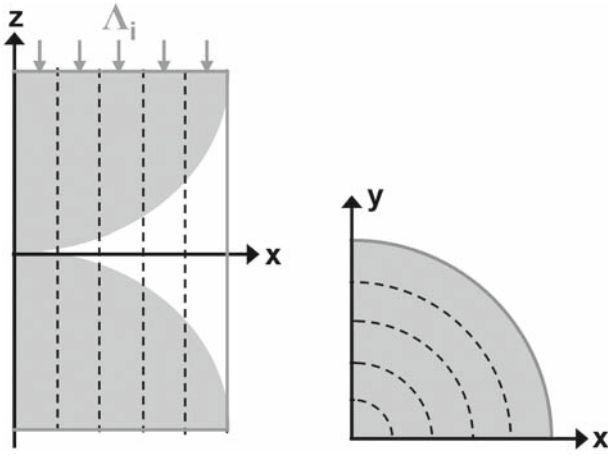

Fig. 3 Cylindrical unit cell for calculating the thermal coupling between the gas phase and the solid particles (*left*: side view, *right*: top view). The cell was divided into 1000 hollow cylinders (the sketch contains only five). Λ_i is the heat transmission coefficient in the hollow cylinder with index i; the direction of the heat flux is indicated by the arrows

tances of the gas phase and solid phase in each hollow cylinder. The resulting heat transmission coefficients Λ_i (in $\mathrm{W \cdot K^{-1}}$) of all hollow cylinders are connected in parallel. Consequently, λ_c is given by

$$\begin{aligned}\lambda_c &= (1-\Pi)\frac{2R}{R^2\pi}\sum_{i=1}^{1000}\Lambda_i \\ &= (1-\Pi)\frac{2R}{R^2\pi}\sum_{i=1}^{1000}\left(\frac{D_i}{\lambda_{g,i}A_i}+\frac{y_i}{\lambda_{\mathrm{part}}A_i}\right)^{-1},\end{aligned} \tag{6}$$

where R is the particle radius; therefore, $2R$ is the height of the unit cell and $R^2\pi$ is its cross-sectional area.

$$y_i = 2\sqrt{R^2-\left(i\frac{R}{1000}\right)^2} \tag{7}$$

is the total height of the solid phase in the hollow cylinder with index i, $D_i = 2R - y_i$ is the corresponding gap size and

$$A_i = \pi\left(i\frac{R^2}{5\times 10^5}+\left(\frac{R}{1000}\right)^2\right) \tag{8}$$

is the ring area of the respective hollow cylinder. The gaseous thermal conductivity $\lambda_{g,i}$ is calculated for each gap size D_i with Eq. 2. The thermal conductivity λ_{part} of the solid particles in RF-aerogel is equal to the thermal conductivity of bakelite, which is about $0.23\,\mathrm{W \cdot m^{-1} \cdot K^{-1}}$ [10].

Unlike Zehner's original model, the aerogel model takes only spherical particles into account; however, SEM pictures show that this approximation is acceptable for aerogels. It has to be pointed out that in addition the parallel heat flow along the z-axis of the unit cell assumed for the derivation of Eq. 6 is only a coarse approximation for the real heat flux lines in the contact region.

3 Experimental

3.1 Thermal-Conductivity Measurements

The effective thermal conductivity was determined by applying the hot-wire method [11]. For this purpose, a platinum wire with a diameter of 100 μm is embedded between two half cylinders of the aerogel samples along the center axis of the cylinder. The wire is heated with a constant electrical power, and the temperature increase of the wire is determined using the relationship between the specific electrical resistance of platinum and the temperature. Finally, the total effective thermal conductivity can be derived by fitting a theoretical solution for the time-dependent temperature increase

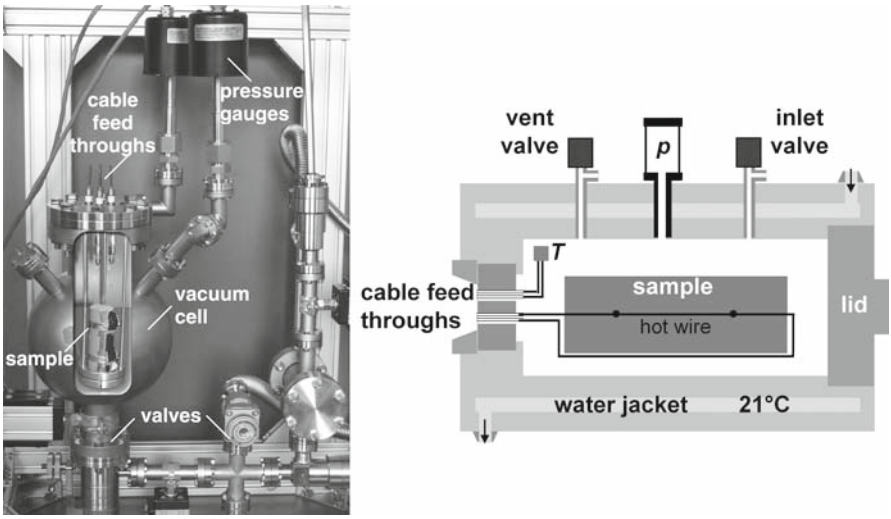

Fig. 4 Experimental setup; *left*: high vacuum arrangement, *right*: high pressure cell

of the hot wire on the experimentally derived data by applying a nonlinear regression routine [12]. The solution used takes into account heat losses of the hot wire via the supply leads and a possible thermal contact resistance between the wire and the sample.

For gas pressures below 0.1 MPa, the hot-wire experiment was performed in a high vacuum setup (see Fig. 4, *left*). This setup was placed in a climatic chamber to control the temperature during the experiment at 21 °C. Different gas pressures were realized by venting the evacuated cell with a defined amount of gas. The gas pressure was determined in the range from 10 Pa to 0.1 MPa by using two membrane pressure transducers (Type MKS Baratron, range of 100 Pa and 0.1 MPa, resolution of 0.01 Pa and 10 Pa, respectively).

For thermal-conductivity measurements at higher gas pressures up to 10 MPa, a temperature-controlled pressure cell (autoclave) was used. The vessel was also kept at a constant temperature of 21 °C, using a water-filled jacket connected to a thermostat. The gas pressure was measured with one membrane pressure transducer of 16 MPa range and a resolution of 0.04 MPa. The experimental setup is depicted in Fig. 4 (*right*).

3.2 Probing Gases

Two different gases, argon (purity of 0.99999) and helium (purity of 0.99999), were used as pore gases. The relevant physical properties are compiled in Table 1. All values for helium, i.e., mean free path, thermal conductivity, and specific heat, clearly exceed the corresponding data of argon. Since helium and argon are inert gases, effects due to adsorption at the inner surface of the aerogels can be neglected. At gas pressures above 0.1 MPa, the thermal conductivities of the free gases strongly increase with increasing

Table 1 Physical properties, i.e., mean free path l_g, thermal conductivity of the free gas $\lambda_{g,0}$, and specific heat c_V, of argon and helium at ambient conditions ($T = 300$ K, $p_g = 0.1$ MPa) [13,14]

Gas	l_g (nm)	$\lambda_{g,0}\left(\mathrm{W \cdot m^{-1} \cdot K^{-1}}\right)$	$c_V\left(\mathrm{J \cdot kg^{-1} \cdot K^{-1}}\right)$
Argon	64	0.017	317
Helium	180	0.154	3210

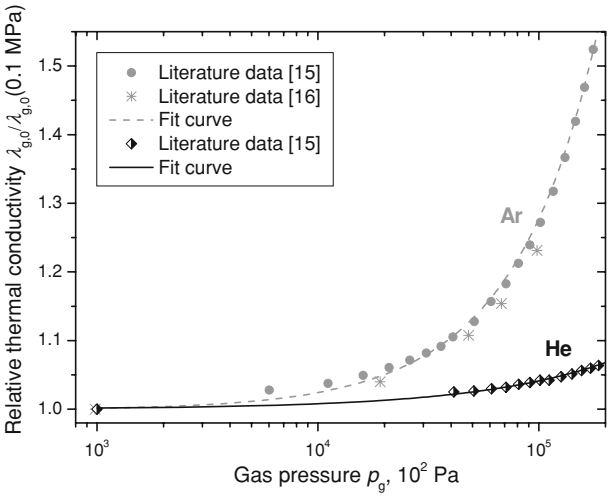

Fig. 5 Thermal conductivities of free argon and helium as a function of gas pressure normalized to the respective thermal conductivities at 0.1 MPa. Experimental data were taken at room temperature [15,16]. The lines represent fit curves to the data, that were later used for calculation of the theoretical gaseous contribution to the total thermal conductivity by Eq. 2

gas pressure (Fig. 5). Particularly, the argon curve reveals a steep increase at high gas pressures.

3.3 Samples Investigated

Two organic aerogel samples with different average pore sizes were investigated. They were synthesized via a sol–gel process [17], starting with an aqueous solution of resorcinol and formaldehyde [18]. The addition of a basic catalyst controls the sol–gel transition in which sol particles occur and interconnect to form a cross-linked polymer network (see Fig. 1), the wet gel. In order to provide a porous solid, the gel is dried via evaporation of the pore liquid at ambient conditions. To reduce the capillary forces and therefore the amount of shrinkage upon drying, the water in the wet gel was exchanged for ethanol prior to starting the drying step.

The two sample types were prepared with almost the same densities and porosities, however, different average pore sizes of 0.6 μm and 7 μm (see Table 2). Within the framework of this paper, the two samples are denoted as RF0.6 and RF7, respectively.

Table 2 Properties of the RF-aerogels investigated

Sample	$\rho_a\,(g\cdot cm^{-3})$	Φ (%)	Π (%)	d_{part} (μm)	D_{pore} (μm)	$S_{BET}\,(m^2\cdot g^{-1})$	$S_{ext}\,(m^2\cdot g^{-1})$
RF0.6	0.33	78	67	0.2	0.6	32.2	15.9
RF7	0.32	79	69	3	7	–	1.33

ρ_a, aerogel density; Φ, measured porosity; Π, corrected porosity (Eq. 5); d_{part}, particle diameter; D_{pore}, pore diameter; S_{BET} and S_{ext}, specific surface areas determined by nitrogen sorption measurements

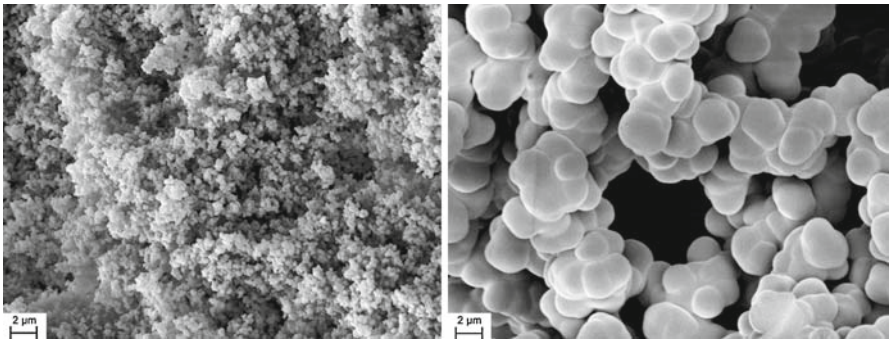

Fig. 6 SEM pictures of the RF-aerogel samples investigated; *left*: RF0.6, *right*: RF7. Note that both pictures were taken at the same magnification

The different structural dimensions of the two samples can be seen in the SEM pictures in Fig. 6.

The specific surface areas, S_{BET} and S_{ext}, given in Table 2 were obtained from nitrogen sorption measurements. While S_{BET} represents the total specific surface area determined via the BET model [19], the external surface area S_{ext}, which is derived via the so-called t-plot [19], is the area of all pores larger than 2 nm. Assuming cylindrical pores, the mean pore size D_{pore} can be derived from the external surface area S_{ext}, the sample density ρ_a, and the density of the organic skeleton $\rho_s \approx 1500\ kg\cdot m^{-3}$ [20], using the relation $D_{pore} = 4(1/\rho_a - 1/\rho_s)/S_{ext}$. For pores larger than 1 μm like in the case of sample RF7, the specific surface area is very small and therefore cannot be measured very accurately. In this case, S_{ext} was determined from the mean particle diameter d_{part}, which was estimated using the SEM pictures; assuming a spherical particle geometry, the following relationship holds: $S_{ext} = 6/(d_{part}\rho_s)$.

4 Results

Figure 7 shows the experimentally determined total thermal conductivity as a function of gas pressure of the two aerogel samples investigated, both measured in argon and helium at a temperature of 21 °C. At high gas pressures, the helium curves reach a level up to four times higher than the argon data. This is due to the extremely high thermal conductivity of free helium (Table 1). In all cases, the gas contribution to the total thermal conductivity clearly exceeds $\lambda_{g,0}$ at high gas pressures. This indicates

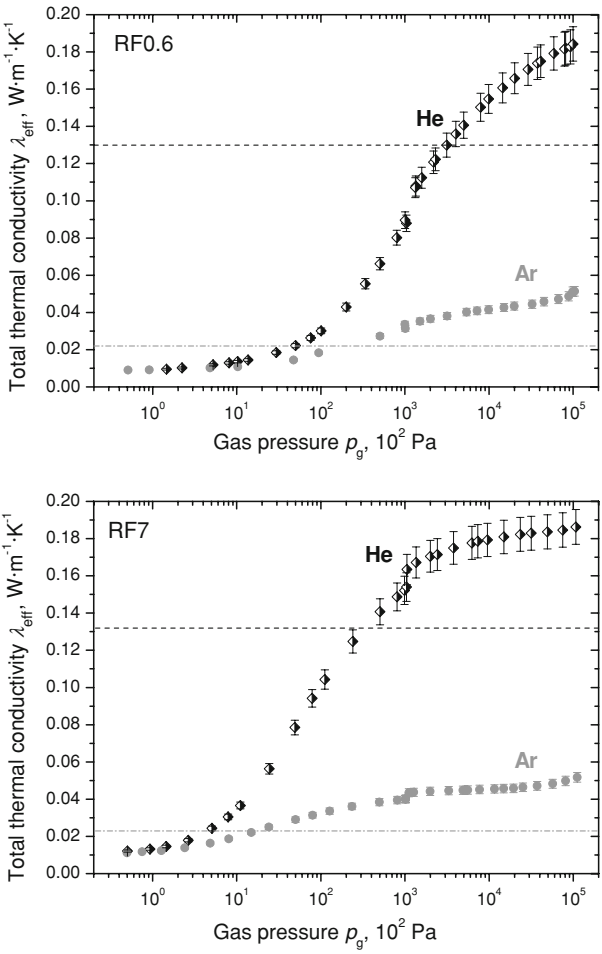

Fig. 7 Measured total thermal conductivities for both aerogels and gases as a function of gas pressure at a temperature of 21 °C. *Dashed black lines* mark the position $\lambda_s + \lambda_r + \Phi\lambda_{g,0,He}$(300 K, 0.1 MPa); *grey lines* including *dashes* and *dots* represent $\lambda_s + \lambda_r + \Phi\lambda_{g,0,Ar}$(300 K, 0.1 MPa)

that even in aerogels, thermal coupling between the solid particles and the gas phase is significant.

For RF0.6 and RF7, the inflection points of the thermal conductivities in the half-logarithmic representation are clearly located at different pressures. On the other hand, the offset of the *s*-curve, which describes the combined contribution of solid and radiative conductivities, is almost equal for both samples; this is expected because of the very similar densities and extremely high extinction coefficients [21].

The jump in all measured curves at 0.1 MPa is caused by the two different experimental setups used below and above ambient pressure. By evacuating the vacuum chamber, adsorbed water molecules can be removed easily from the aerogel backbone. However, flushing the sample in the autoclave with the probing gas for several hours does not yield the same efficiency. Therefore, the data taken above 0.1 MPa

include an offset, which is probably caused by thermal bridging via adsorbed water. This is proved by the fact that venting and refilling of the autoclave reduces the thermal conductivity value at a certain gas pressure. The amount of the offset, i.e., the difference between the results measured with both setups at 0.1 MPa, is on the order of $0.01\,\mathrm{W \cdot m^{-1} \cdot K^{-1}}$ for helium and $0.002\,\mathrm{W \cdot m^{-1} \cdot K^{-1}}$ for argon.

The error bars in Fig. 7 represent the expanded standard measurement uncertainty. Uncertainties due to a temperature fluctuation of about ±0.5 K were estimated to be negligible.

5 Discussion

The first increase in λ_{eff} at gas pressures of about 10 Pa to 50×10^2 Pa is due to the gaseous conduction in the interparticle pores, $\lambda_{\mathrm{g,pore}}$. According to the theory (see Eq. 2), the corresponding inflection point depends on the average pore size and the mean free path of the probing gas. For a given probing gas, the curve for sample RF7 is, therefore, expected to be shifted by about a factor of ten to lower gas pressures in contrast to sample RF0.6; a comparison of the two plots in Fig. 7 shows that the expected shift is actually observed. Comparing the experimental curves for a given sample but different gases (e.g., Figs. 8 and 9), reveals a shift of the inflection point to lower gas pressures for argon in comparison to helium. This corresponds to the effect predicted by Eq. 2 in combination with the different characteristic mean free paths (Table 1). Theoretically, the amount of the shift is equal to the factor by which the mean free paths differ. That means, in the case of argon and helium, a shift by a factor of three in gas pressure can be expected. This quantitative behavior is also confirmed by the experimental results.

For high gas pressures ($p_{\mathrm{g}} > 10^4$ Pa), the height of the expected s-shaped thermal-conductivity curves is mainly determined by the coupling effect, i.e., the thermal

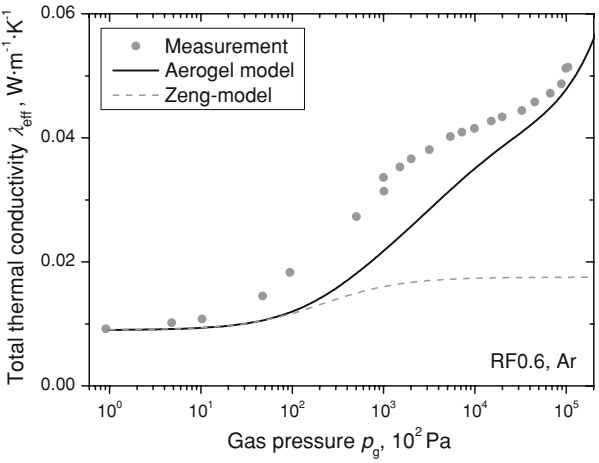

Fig. 8 Comparison of the experimentally derived thermal-conductivity values for sample RF0.6 in an argon atmosphere with theoretical values predicted by the model of Zeng et al. [2] and the aerogel model

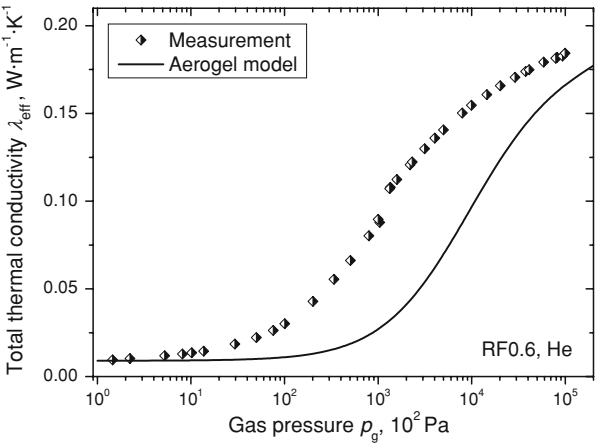

Fig. 9 Comparison of the experimentally derived thermal-conductivity values for sample RF0.6 in a helium atmosphere with theoretical values predicted by the aerogel model

bridging in the vicinity of the particle contacts. However, the typical pronounced plateau is not present. The experimental data rather exhibit a slightly increasing slope. On the one hand, this is a result of the continuously decreasing gap sizes between the particles, starting from the edge of the unit cell. When probing with growing gas pressure, each gap size contributes to the heat transfer in the aerogel at another gas pressure according to Eq. 2. This effect generally leads to a broadening of the transition region in the *s*-curve. In addition, the gas pressure dependence of $\lambda_{g,0}$ has to be taken into account (compare Fig. 5), which shows a significant increase of the thermal conductivity for gas pressures above 1 MPa, especially in the case of argon. The last steep increase in the argon curves results from this behavior.

In Figs. 8, 9, 10, and 11 the experimental data are compared to the theoretical predictions by the aerogel model; hereby, the structural parameters listed in Table 2 were used. In Fig. 8, the theoretically expected curve according to the model by Zeng et al. [2] (see Eq. 1) is exemplarily plotted in addition. The model of Zeng et al. shows a large deviation from the measured curve, in particular, at high gas pressures, because the gas pressure dependence of $\lambda_{g,0}$ and the coupling effect are neglected.

All curves calculated via the aerogel model show a similar shape for the experimental data plotted versus the gas pressure. However, the experimental data seem to be shifted by about a factor of 10 toward lower gas pressures compared to the theoretical predictions. This means that the pore size values, derived from both nitrogen sorption and SEM pictures, are about a factor of 10 smaller than the effective pore sizes relevant for the heat transfer in aerogels. Moreover, the particle sizes taken from the SEM pictures seem to be too small.

6 Conclusion and Outlook

The first pressure-dependent thermal-conductivity measurements on highly porous materials with pores <10 μm, i.e., RF-aerogels, were performed over six pressure

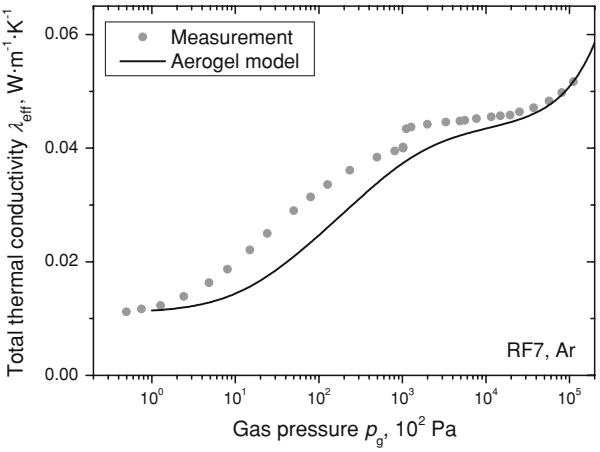

Fig. 10 Comparison of the experimentally derived thermal-conductivity values for sample RF7 in an argon atmosphere with theoretical values predicted by the aerogel model

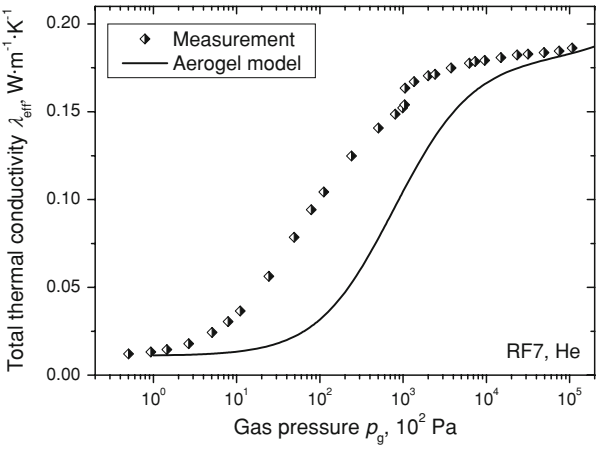

Fig. 11 Comparison of the experimentally derived thermal-conductivity values for sample RF7 in a helium atmosphere with theoretical values predicted by the aerogel model

decades up to 10 MPa. The results provide important information about heat transfer in RF-aerogels at high gas pressures. The thermal coupling between the gas phase and the solid particles is significant in the RF-aerogels investigated and cannot be neglected. It is expected that the derived results can also be observed for other nanoporous materials.

In order to get a better understanding of the interaction of the different heat transfer mechanisms, the established Zehner model was modified and compared to the experimental thermal-conductivity curves as a function of gas pressure. Good qualitative agreement was observed, i.e., the influence of the interparticle pores, the coupling effect, and the gas–pressure dependence of the free gas at high pressure can be modeled qualitatively. A quantitatively correct description by this model, however, failed.

It seems that an effective pore size model is not sufficient to describe the heat transfer. Therefore, in the future a more appropriate model which includes different pore sizes ("multi-scale model") needs to be developed. In addition, further nanoporous model systems, e.g., pyrogenic silica, and gases, like CO_2 and N_2, will be investigated. Since gas-pressure-dependent thermal-conductivity measurements can be used as a convenient and non-destructive characterization method for nanoporous systems, it is of importance that a reliable description of the heat transfer within these systems is available, also at high gas pressures.

Acknowledgments The authors would like to thank Mr. M. Geis for the preparation of the samples, as well as Ms. E. Langholf and Ms. D. Winkler for support during the thermal-conductivity measurements.

References

1. G. Reichenauer, H.-P. Ebert, The Nanotech J. **01.08**, 17 (2008)
2. S.Q. Zeng, A. Hunt, R. Greif, J. Non-Cryst. Solids **186**, 264 (1995)
3. G. Reichenauer, U. Heinemann, H.-P. Ebert, Colloid Surf. A **300**, 204 (2007)
4. G. Reichenauer, Aerogels. in *Kirk-Othmer Encyclopedia of Chemical Technology* (John Wiley & Sons, Inc., New York, 2008)
5. J. Fricke, High Temp.-High Press. **25**, 379 (1993)
6. M.G. Kaganer, *Thermal Insulation in Cryogenic Engineering* (IPST Press, Jerusalem, Israel, 1969)
7. X. Lu, P. Wang, M.C. Arduini-Schuster, J. Kuhn, D. Büttner, O. Nilsson, U. Heinemann, J. Fricke, J. Non-Cryst. Solids **145**, 207 (1992)
8. R.W. Pekala, C.T. Alviso, X. Lu, J. Gross, J. Fricke, J. Non-Cryst. Solids **188**, 34 (1995)
9. P. Zehner, E.U. Schlünder, Chem. Ing. Tech. **44**, 1303 (1972)
10. H. Kuchling, *Taschenbuch der Physik* (Fachbuchverlag Leipzig, München, Wien, 1999)
11. B. Stalhane, S. Pyk, Teknisk Tidskrift **61**, 389 (1931)
12. H.-P. Ebert, V. Bock, O. Nilsson, J. Fricke, High Temp.-High Press. **25**, 391 (1993)
13. W. Umrath, *Fundamentals of Vacuum Technology* (Leybold AG, Cologne, 1998)
14. H. Reiss, *VDI-Wärmeatlas* (Springer-Verlag, Berlin, Heidelberg, 1997)
15. J. Kestin, R. Paul, A.A. Clifford, W.A. Wakeham, Physica **100 A**, 349 (1980)
16. B.J. Bailey, K. Kellner, Physica **39**, 444 (1968)
17. R.W. Pekala, F.M. Kong, A synthetic route to organic aerogels—mechanism, structure and properties. in *Proceedings of 2nd Int. Symp. on Aerogels* (1989), pp. C4-33–C4-40
18. M. Wiener, G. Reichenauer, T. Scherb, J. Fricke, J. Non-Cryst. Solids **350**, 126 (2004)
19. K.S.W. Sing, D.H. Everett, R.A.W. Haul, L. Moscou, R.A. Pierotti, J. Rouquerol, T. Siemieniewska, Pure Appl. Chem. **57**, 603 (1985)
20. G. Reichenauer, C. Stumpf, J. Fricke, J. Non-Cryst. Solids **186**, 334 (1995)
21. X. Lu, M.C. Arduini-Schuster, J. Kuhn, O. Nilsson, J. Fricke, W. Pekala, Science **255**, 971 (1992)